

MODELING A 5-DOF HAPTIC INTERFACE FOR ISOTROPIC FORCE CONTROL

Christopher D. Lee^a, Dale A. Lawrence^{b,1}, and Lucy Y. Pao^a

^a*Electrical & Computer Engineering Department,
University of Colorado, Boulder, CO 80309-0425*

^b*Aerospace Engineering Sciences Department,
University of Colorado, Boulder, CO 80309-0429*

toph@colorado.edu, dale.lawrence@colorado.edu, and
pao@colorado.edu

Abstract:

This paper describes a multivariable modeling and control strategy that increases the bandwidth of isotropic force transmission in multi-degree of freedom haptic interfaces. The controller structure leads to a straightforward model identification procedure and yields a simple control law that can be easily implemented. Experimental results show that this technique significantly improves force tracking performance on a 5 degree-of-freedom in-parallel haptic interface.

Classification codes: A1 and G1

Keywords: force control, modeling, haptic interfaces, multi-input multi-output, parameter identification, weighted least squares

1. INTRODUCTION

Haptic interfaces provide forces on a user's hand in response to hand motion. These forces can be actual forces transmitted from a remote location, as in teleoperation applications, or forces produced by a model in a computer, as in virtual reality applications. A five degree-of-freedom (DOF) haptic interface has been developed at the University of Colorado (CU), as shown in Figure 1, for use in scientific visualization of 3-dimensional data fields, and in learning and communicating 3-dimensional spatial concepts.

An ideal haptic interface should have a large range of motion in multiple degrees of freedom, low friction and mass, and accurate transmission of desired forces from the remote or virtual environment to the user. This paper focuses on high-fidelity force transmission to the user's fingers. Although the human hand's sensitivity to vibration reaches its maximum at about 300 Hz (Bolanowski *et al.*, 1988), such high bandwidth



Fig. 1. Parallel haptic interface with 5 prismatic actuators connected to a hand-held stylus.

may not be as important in a haptic interface as a moderate bandwidth, but with equal (isotropic) force tracking fidelity in all degrees of freedom.

This paper discusses a multi-input multi-output (MIMO) modeling and control design strategy that can increase the bandwidth of rendered forces equally in all degrees of freedom, despite kinematic and dynamic anisotropy in the

* This work was supported in part by the National Science Foundation (IIS-9711936 and HRD-0095944) and the Office of Naval Research (N00014-97-1-0354).

† Corresponding author. FAX +1 (303) 492-7881 Phone +1 (303) 492-3025.

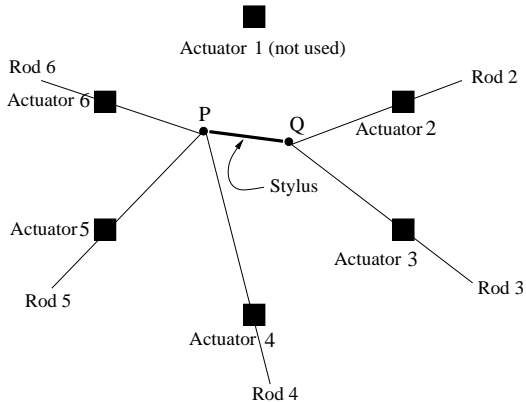


Fig. 2. Diagram of the haptic interface.

haptic interface. This method seeks as simple a model as possible for the dynamics of a multivariable force control loop and uses a robust identification method to yield a relatively simple multivariable control law that can be easily implemented.

This paper is organized as follows. The haptic interface used is described in more detail in Section 2. Section 3 outlines the performance measures and control strategy. Section 4 overviews a parameter identification technique that yields a model that can be used for the inverse model control strategy. Section 5 discusses a scalar compensator used to stabilize the system and presents closed-loop control results.

2. HAPTIC INTERFACE DESCRIPTION

The CU haptic interface (Figures 1 and 2) was designed to promote high fidelity force sensing and transmission to the user in 3 DOF in translation and 2 DOF in rotation (Lee *et al.*, 2000). Each link consists of a thin rod controlled by a prismatic friction drive actuator. Actuators are attached to a hexagonal base via two-DOF gimbals. The hand grip is a pen shaped stylus attached to three actuator rods on one end and two rods on the other. Each rod attaches to the stylus through a three axis gimbal. Force sensors are located at the tip of each rod to provide feedback of measured axial rod forces to the force control loop. Accurate transmission of sensed forces to the user's fingers is provided by light, stiff connections between the stylus and these sensors. Optical encoders embedded in the actuators measure rod displacement. A DSP computer running between 1-2 kHz loop rates (depending on the application) implements the force control law, in addition to performing the required kinematic transformations and data interpolation to render desired effects as the user investigates data, *e.g.*, for scientific visualization of vector fields (Lawrence *et al.*, 2000).

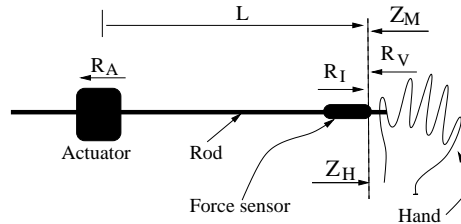


Fig. 3. Hand/Mechanism partition, actuator force R_A , measured rod axial force R_I , and rod length L for a one-rod case.

2.1 Mathematical Description

There is a natural separation of the haptic interface dynamics into a component representing the interface mechanism itself, and a component representing the user's hand. Figure 3 shows this partition for a single rod case, as well as the location of actuator forces R_A , sensed (mechanism/hand interaction) forces R_I , voluntary user forces R_V , and measured rod length L . In the multiple-rod case, the force sensors induce an unusual partition of mechanism and hand dynamics that is expedient for model identification. Here, the Mechanism impedance, Z_M , includes all hardware up to the force sensors, whereas the Hand impedance, Z_H , includes all dynamics outboard of the force sensors, *i.e.*, the stylus, rod tip gimbals, and user's hand lumped together.

Figure 4 shows the 5-DOF force control loop resulting from the attachment of the five rods to the stylus and hand. Forces and motions are described not in Cartesian coordinates, but along the 5 moving rod axes. G is the force controller.

This force loop is designed to cause the five-tuple of measured rod interaction forces, R_I , to track the five force loop commands (desired forces) R_D , using the multivariable control law G , which outputs five actuator forces, R_A . The R_I are measurements of interaction forces along each rod's long axis. Motion of the Mechanism causes changes in the distance between each actuator and the end of the rod. The 5-tuple of these rod lengths is denoted L . Changes in L cause a reaction force from the Hand, denoted R_H , due to the impedance of the Hand, Z_H . This reaction force and the voluntary user force R_V combine to form the interaction force R_I . In turn, the motion L results from the sum of actuator forces R_A and interaction forces R_I acting on the Mechanism admittance Z_M^{-1} .

When the user does not supply any voluntary forces (*i.e.*, $R_V = 0$), the block diagram of Figure 4 yields

$$\begin{aligned} R_I(s) &= -Z_H(s)L(s) \\ R_I(s) - R_A(s) &= Z_M(s)L(s) \\ R_A(s) &= -Z_T(s)L(s) \end{aligned} \quad (1)$$

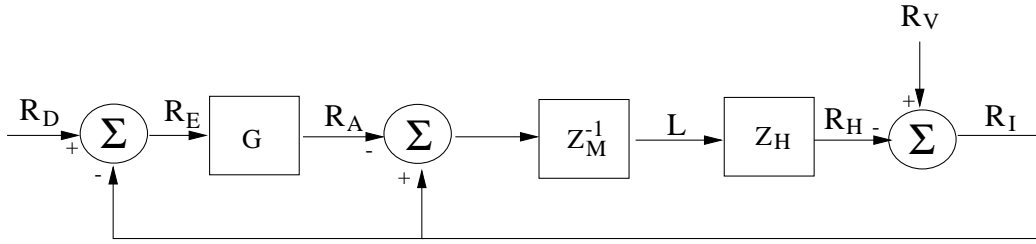


Fig. 4. Overall control structure with separate Hand and Mechanism impedances.

where $Z_T(s)$ is the Total interface impedance $Z_T(s) = Z_M(s) + Z_H(s)$. The relation between actuator forces R_A and measured interaction forces R_I is the “plant”, $P(s)$, used for subsequent control design:

$$\begin{aligned} R_I(s) &= P(s) R_A(s) \\ P(s) &= Z_H(s) (Z_T^{-1}(s)). \end{aligned} \quad (2)$$

This decomposition into a Mechanism and Hand impedance, and the corresponding modeling and control methods discussed here, are applicable to any haptic interface, whether parallel, serial, or serial-parallel in design. Ideally, the force sensing should be located as close to the user’s fingers as possible, so that the measured forces closely represent those felt by the user, and so that the force loop causes these to track the desired forces.

3. PERFORMANCE MEASURES AND CONTROL STRATEGY

3.1 Performance Measures

The goal of the force controller is to increase the bandwidth of isotropic force transmission. Typically, this is a multivariable (MIMO) controller, since SISO control is extremely limited in its ability to affect isotropy. The force transmission transfer function $T(j\omega)$ relating desired forces R_D to interaction forces R_I can be derived from the block diagram in Figure 4 and equation (2):

$$\begin{aligned} R_I(j\omega) &= T(j\omega) R_D(j\omega) \\ T(j\omega) &= (I + P(j\omega) G(j\omega))^{-1} P(j\omega) G(j\omega). \end{aligned}$$

Ideally, $T(j\omega) = I$, so that the user feels the desired force R_D in all degrees of freedom. This can sometimes be achieved (typically only at low frequencies) by a minimum singular value $\underline{\sigma}(P(j\omega) G(j\omega))$ which is large compared to 1. At higher frequencies, $\underline{\sigma}(P(j\omega) G(j\omega))$ necessarily becomes smaller to ensure stability. When the condition number of $P(j\omega) G(j\omega)$ is large, the minimum and maximum singular values are widely separated, resulting in a wide variation in loop gain in different directions. As a result, the

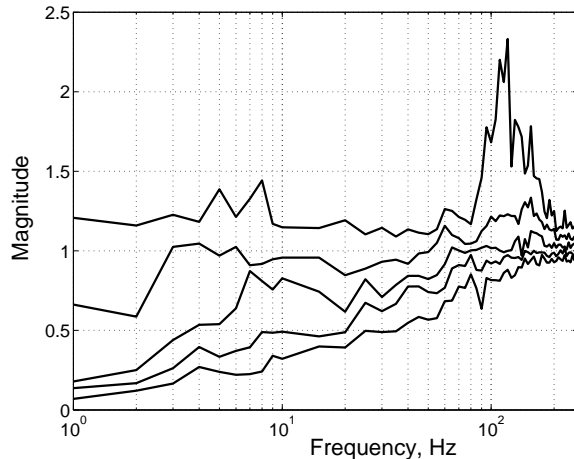


Fig. 5. Singular values of $(T(j\omega) - I)$ under SISO control.

rendered force vector may be corrupted in magnitude and/or direction. Therefore, we seek to reduce the condition number of $P(j\omega) G(j\omega)$, particularly at frequencies where $\underline{\sigma}(P(j\omega) G(j\omega))$ is near 1. This extends the bandwidth of isotropic force tracking, and simultaneously promotes better stability margins.

A performance measure should quantify both the correctness of magnitude and *direction* of rendering. Hence, we define the bandwidth of isotropic force tracking as the maximum frequency where $\bar{\sigma}(T(j\omega) - I)$ is less than $1 - 1/\sqrt{2} \approx 0.293$ (analogous to the 3 dB bandwidth definition for scalar systems). Figure 5 shows the singular values of $(T(j\omega) - I)$ under a SISO controller. Note that the vertical axis is magnitude (not in dB), so these should ideally be 0. The isotropic force transmission bandwidth (as defined above) is less than 1 Hz, with wide directional variation at low frequencies. Multivariable control will be applied to improve isotropic bandwidth by “compressing” singular values together, reducing the condition number. In our method, stability of the force loop is assessed using the multivariable Nyquist criterion (MacFarlane *et al.*, 1977). This multivariable version of the Bode and Nyquist analyses uses the eigenvalues of the loop transfer function matrix, counting encirclements of the critical point in a similar way as for scalar systems. Gain and phase margins can be similarly inferred, provided that the eigenvectors are nearly orthogonal. We have

used a gain margin of about 6 dB and phase margin of 30 degrees, but larger margins may be in order when models are poor.

3.2 Control Strategy

Given the objective of “compressing” the singular values of the loop gain, an inverse model control strategy is pursued. If $\hat{Z}_H(s)$ and $\hat{Z}_T(s)$ are models of the Hand and Total impedances respectively, then a MIMO controller can take the form:

$$R_A(s) = G(s) R_E(s)$$

with

$$G(s) = g(s) \hat{Z}_T(s) \hat{Z}_H^{-1}(s) = g(s) \hat{P}^{-1}(s) \quad (3)$$

where $\hat{P}^{-1}(s)$ is the plant model and $g(s)$ is a simple scalar compensator used to further shape the frequency response by increasing low-frequency gain and providing roll-off at higher frequencies. To the extent that the plant model matches the plant, the singular values of $P(s) \hat{P}^{-1}(s)$ will be compressed into a narrow band around 0 dB, allowing force tracking to be similarly effective in all directions. The second-order polynomial forms used for the impedances in \hat{P} (see below) are well-suited to model inversion, since the resulting model has relative degree zero, and the inverse is realizable without large high frequency gains.

4. MODELING

The goal of this section is to obtain a parametric model of the plant transfer function of the form:

$$\hat{P}(s) = \hat{Z}_H(s) \hat{Z}_T^{-1}(s). \quad (4)$$

To this end, we first seek separate Mechanism and Hand impedance models. Previous work (Lee *et al.*, 2002) suggests that a second-order linear model of the Mechanism provides considerable accuracy in modeling the non-Coulomb friction portion of the Mechanism dynamics at low frequencies. The model was of the form:

$$\hat{Z}_M(s) = \hat{M}_M s^2 + \hat{B}_M s + \hat{K}_M.$$

In this paper we will examine the feasibility and performance of Hand and Total impedance models of the same form:

$$\begin{aligned} \hat{Z}_H(s) &= \hat{M}_H s^2 + \hat{B}_H s + \hat{K}_H \\ \hat{Z}_T(s) &= \hat{M}_T s^2 + \hat{B}_T s + \hat{K}_T. \end{aligned} \quad (5)$$

Although the Hand is undoubtedly more complex than a second-order model, and may be better modeled with a non-linear time-varying model, it will be shown that the second-order model greatly improves controller design. The mass matrices

\hat{M}_H and \hat{M}_T , damping matrices \hat{B}_H and \hat{B}_T , and stiffness matrices \hat{K}_H and \hat{K}_T will be obtained using a least squares fitting of frequency domain data in Section 4.2 using the equations in (1).

4.1 Hand and Total Impedance Frequency Response Data

Here we discuss only the Hand; the method for the Total impedance is identical. The relationship at a frequency ω between interaction forces R_I and rod displacements L is

$$R_I(j\omega) = -Z_H(j\omega) L(j\omega).$$

Let $Z_H(j\omega) = [z_{ij}(j\omega)]$. $z_{ij}(j\omega)$ relates the j th rod length L^j to the i th interaction force R_I^i . To obtain the scalar frequency responses of the z_{ij} at a set of frequencies $[\omega_1, \omega_2, \dots, \omega_N]$, the system must be excited at those frequencies. Let $R_A(t)$ denote the 5-tuple of actuator input forces at time t , and consider the following five sets of actuator inputs over a time period τ , to be used in a set of five data collection experiments:

$$\begin{aligned} R_{A_1}(t) &= r_f(t) [-1 \ 1 \ 1 \ 1 \ 1]^T \\ R_{A_2}(t) &= r_f(t) [1 \ -1 \ 1 \ 1 \ 1]^T \\ R_{A_3}(t) &= r_f(t) [1 \ 1 \ -1 \ 1 \ 1]^T \\ R_{A_4}(t) &= r_f(t) [1 \ 1 \ 1 \ -1 \ 1]^T \\ R_{A_5}(t) &= r_f(t) [1 \ 1 \ 1 \ 1 \ -1]^T \end{aligned} \quad (6)$$

where $r_f(t)$ is a pseudo-random signal

$$r_f(t) = \sum_{k=1}^N a \cos(\omega_k t + \alpha_k)$$

and the α_k are uniformly distributed random phases in the interval $[0, 2\pi]$. a is selected to produce an adequate signal to noise ratio in measured data. If N is the number of time samples during an experiment of length τ seconds, *i.e.*, $\tau = N t_s$ with t_s being the sample period, then the frequencies ω_k must be integer multiples of $\frac{2\pi}{t_s}$ to avoid errors in the FFT. For each experiment (for $\ell = 1, \dots, 5$), by taking the Fast Fourier Transform (FFT) of the measured forces and rod lengths, one obtains¹, at each frequency ω :

$$\begin{aligned} R_{I_\ell}(j\omega) &= \begin{bmatrix} R_{I_\ell^2}^2(j\omega) \\ R_{I_\ell^3}^3(j\omega) \\ R_{I_\ell^4}^4(j\omega) \\ R_{I_\ell^5}^5(j\omega) \\ R_{I_\ell^6}^6(j\omega) \end{bmatrix} = -Z_H(j\omega) \begin{bmatrix} L_\ell^2(j\omega) \\ L_\ell^3(j\omega) \\ L_\ell^4(j\omega) \\ L_\ell^5(j\omega) \\ L_\ell^6(j\omega) \end{bmatrix} \\ &\Rightarrow R_{I_\ell}(j\omega) = -Z_H(j\omega) L_\ell(j\omega). \end{aligned}$$

¹ The superscript in $R_{I_\ell}^m$, $m = 1, \dots, 5$ is used to index rod number and is not a power exponent.

By concatenating these results by column into matrix form, one obtains

$$\mathcal{R}_I(j\omega) = -Z_H(j\omega) \mathcal{L}(j\omega) \quad (7)$$

where

$$\begin{aligned} \mathcal{R}_I(j\omega) &= [R_{I_1}(j\omega) \ R_{I_2}(j\omega) \ \cdots \ R_{I_5}(j\omega)] \\ \mathcal{L}(j\omega) &= [L_1(j\omega) \ L_2(j\omega) \ \cdots \ L_5(j\omega)] \end{aligned}$$

are both 5×5 matrices at each frequency ω . Hence, the empirical (measured) impedance $Z_H(j\omega)$ can be found as

$$Z_H(j\omega) = -\mathcal{R}_I(j\omega) \mathcal{L}(j\omega)^{-1}$$

provided the columns of \mathcal{L} are linearly independent. In our experiments, the choice (6) provided sufficiently independent columns in \mathcal{L} . Other choices are possible, but the particular choice of $R_{A_i}(t)$ affects the quality of the frequency response: if one of the rods is not sufficiently actuated, data will be corrupted by quantization noise, friction, *etc.* This is most likely to occur at high frequencies when the amplitude of motion is reduced and friction may dominate. We observed this deficiency, for example, when only one rod was excited at a time. This caused so little motion in some rods that the empirical impedance was highly inaccurate.

After constructing a similar model for Z_T , we fit parameterized models, corresponding to mass, spring, and damping matrices.

4.2 M, B, K Model of Z_H and Z_T

Again, we discuss the method only for the Hand, the method for Total impedance being similar. For each element $z_{ij}(j\omega)$ of the Hand impedance Z_H , we parameterize as follows:

$$\hat{z}_{ij}(j\omega) = [(j\omega)^2 \ j\omega \ 1] \begin{bmatrix} \hat{m}_{ij} \\ \hat{b}_{ij} \\ \hat{k}_{ij} \end{bmatrix}.$$

Stacking these equations by frequency, we get

$$\hat{Z}_{ij} = \begin{bmatrix} \hat{z}_{ij}(j\omega_1) \\ \hat{z}_{ij}(j\omega_2) \\ \vdots \\ \hat{z}_{ij}(j\omega_N) \end{bmatrix} = \begin{bmatrix} (j\omega_1)^2 & j\omega_1 & 1 \\ (j\omega_2)^2 & j\omega_2 & 1 \\ \vdots & \vdots & \vdots \\ (j\omega_N)^2 & j\omega_N & 1 \end{bmatrix} \begin{bmatrix} \hat{m}_{ij} \\ \hat{b}_{ij} \\ \hat{k}_{ij} \end{bmatrix}$$

which we can rewrite as

$$\hat{Z}_{ij} = \phi^H \theta_{ij},$$

where “ H ” denotes the conjugate transpose. A real parameter 3-tuple estimate $\theta_{ij} = [\hat{m}_{ij}, \hat{b}_{ij}, \hat{k}_{ij}]^T$ can be found using least squares, but first we weight the measured data and the information matrix ϕ with a simple model of the inverse of

the frequency response of the data (see Figure 6) to provide more accurate fits at low frequencies:

$$h(j\omega) = \frac{1}{(j\omega + 7 \cdot 2\pi)^2}.$$

The weighted data is

$$\tilde{Z}_{ij} = \begin{bmatrix} h(j\omega_1) z_{ij}(j\omega_1) \\ h(j\omega_2) z_{ij}(j\omega_2) \\ \vdots \\ h(j\omega_N) z_{ij}(j\omega_N) \end{bmatrix}$$

$$\tilde{\phi}^H = \begin{bmatrix} h(j\omega_1)(j\omega_1)^2 & h(j\omega_1)j\omega_1 & h(j\omega_1)1 \\ h(j\omega_2)(j\omega_2)^2 & h(j\omega_2)j\omega_2 & h(j\omega_2)1 \\ \vdots & \vdots & \vdots \\ h(j\omega_N)(j\omega_N)^2 & h(j\omega_N)j\omega_N & h(j\omega_N)1 \end{bmatrix}.$$

The modified minimization problem can be written as

$$\tilde{\theta}_{ij} = \arg \min \left(\tilde{Z}_{ij} - \tilde{\phi}^H \tilde{\theta}_{ij} \right)^H \left(\tilde{Z}_{ij} - \tilde{\phi}^H \tilde{\theta}_{ij} \right). \quad (8)$$

The least squares solution to this modified problem is (Ljung, 1987)

$$\tilde{\theta}_{ij} = \left(\text{Real} \left(\tilde{\phi} \tilde{\phi}^H \right) \right)^{-1} \text{Real} \left(\tilde{\phi} \tilde{Z}_{ij} \right).$$

Since Z_H and Z_T are each 5×5 matrices, there are 50 scalar impedances to be identified. This parameter identification procedure is therefore repeated to obtain the 50 $\tilde{\theta}_{ij}$ parameter 3-tuples of the Hand and Total impedances.

4.3 Modeling results

Z_H and Z_T were modeled using the method above with excitation at the 28 frequencies 1, \dots , 10 and 15, 20, \dots , 100 Hz. The singular values of Z_H and its model \hat{Z}_H are shown in Figure 6. Those for Z_T and its resulting model \hat{Z}_T are shown in Figure 7. It can be seen from these plots that the impedances are not those of strict second-order matrix polynomials. Nevertheless, this relatively simple approximation is accurate enough to capture salient system dynamics. To see this we look at singular values of $P(j\omega) \cdot \hat{P}^{-1}(j\omega)$, which ideally would all be 1. Figure 8 shows that these singular values occupy a magnitude band in the vicinity of ± 7 dB for frequencies up to 30 Hz. Since the original plant had a singular value span of about 25 – 50 dB for frequencies up to 30 Hz, the pairing of the plant with the inverse described here has reduced plant anisotropy by a factor of 8 to 140 over this frequency range.

5. CONTROL IMPLEMENTATION

The controller takes the form:

$$G(s) = g(s) \hat{Z}_T(s) \hat{Z}_H^{-1}(s).$$

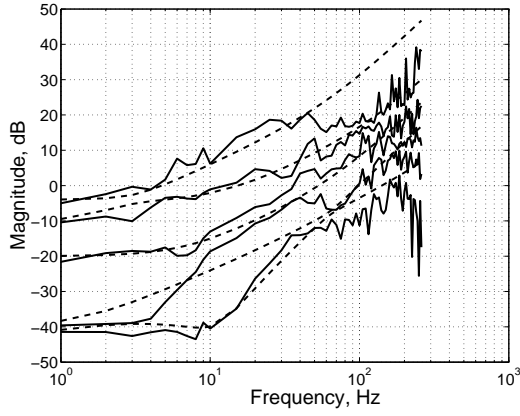


Fig. 6. Singular values of Z_H (solid) and \hat{Z}_H (dashed).

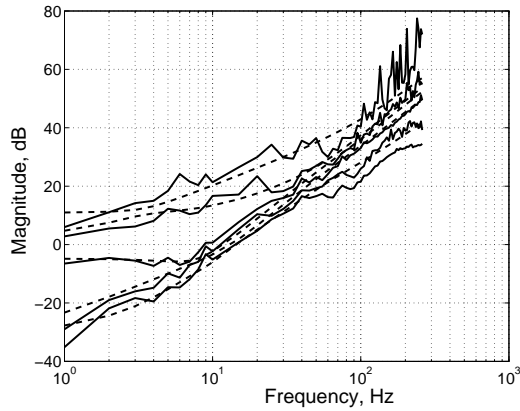


Fig. 7. Singular values of Z_T (solid) and \hat{Z}_T (dashed).

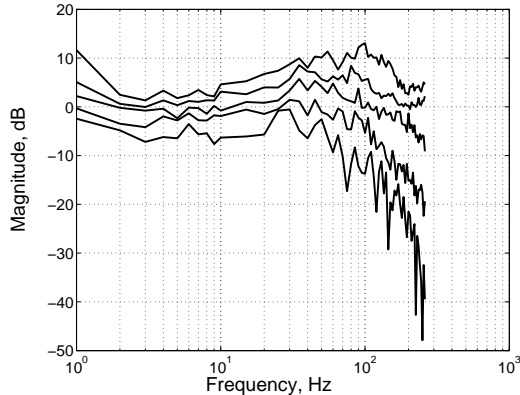


Fig. 8. Singular values of $P \cdot \hat{P}^{-1}$.

which has a simple continuous time implementation. Define $y(s)$ as

$$y(s) = \hat{Z}_T(s)^{-1} R_A(s) = \hat{Z}_H(s)^{-1} g(s) R_E(s).$$

Then,

$$\begin{aligned} g(s) R_E(s) &= \hat{M}_H s^2 y(s) + \hat{B}_H s y(s) + \hat{K}_H y(s) \\ \Rightarrow s^2 y(s) &= g(s) \hat{M}_H^{-1} R_E(s) - \hat{M}_H^{-1} \hat{B}_H s y(s) \\ &\quad - \hat{M}_H^{-1} \hat{K}_H y(s) \end{aligned}$$

and the actuator forces are

$$R_A(s) = \hat{M}_T s^2 y(s) + \hat{B}_T s y(s) + \hat{K}_T y(s).$$

A controller discretization method yielding a simple implementation is discussed in (Lee, 2002). Before addressing the scalar compensator design $g(s)$, we first discuss how to modify right-half-plane poles and zeros which may appear in the model from the least squares parameter matching.

5.1 Right Half Plane Poles and Zeros in Model

The Hand and Total impedances should have zeros in the open complex left half plane (OLHP). Unfortunately, due to noise in the data measurements, the least squares algorithm may return impedance models with zeros in the closed complex right half plane (CRHP). CRHP zeros of $\hat{Z}_H(s)$ cause $G(s)$ to be unstable. This is undesirable since it makes the controller implementation difficult to debug: a frequency response of the controller cannot be obtained before the loop is closed. CRHP roots of $\hat{Z}_T(s)$ cause $G(s)$ to be non-minimum phase and are also undesirable since they induce phase loss with an increase in magnitude, limiting closed-loop bandwidth (Sko-gestad *et al.*, 1996). These two issues can often be remedied by “positizing” the mass, spring, and damping matrices of $\hat{Z}_H(s)$ and $\hat{Z}_T(s)$. If $V D V^{-1}$ is the eigenvector decomposition of a matrix M , then we define M_P to be the positized version of M as follows:

$$M_P = V |D| V^{-1}$$

where $|\cdot|$ is the absolute value of matrix elements.

Once the terms of the impedance model have been positized, the roots of the impedance models $\hat{Z}_H(s)$ and $\hat{Z}_T(s)$ are checked for the presence of remaining CRHP roots. Positizing is usually (but not always) sufficient. One could also symmetrize to *guarantee* OLHP roots (Bellman, 1970), but we have found this can significantly reduce the accuracy of the model \hat{P} , and it is often better to take a new set of data and re-parameterize.

5.2 Scalar Compensator Design

Once the goal of singular value “compressing” is achieved with the inverse model controller, it remains to shape the open-loop frequency response to provide high gain at low frequencies to achieve force transmission, and roll-off at the higher frequencies to subdue unmodeled dynamics. In our work, the scalar $g(s)$ factor was chosen to include a gain, a lag filter to boost low frequency gain, 3 notch filters to address specific peaks in the open-loop response, and 2 low-pass filters to roll off high frequency gain, as follows:

$$g(s) = k \left(\frac{s + z_1}{s + p_1} \right) \prod_{i=1}^3 \left(\frac{s^2 + 2\zeta_1 \omega_i s + \omega_i^2}{s^2 + 2\zeta_2 \omega_i s + \omega_i^2} \right) \prod_{i=2}^3 \left(\frac{p_i}{s + p_i} \right)$$

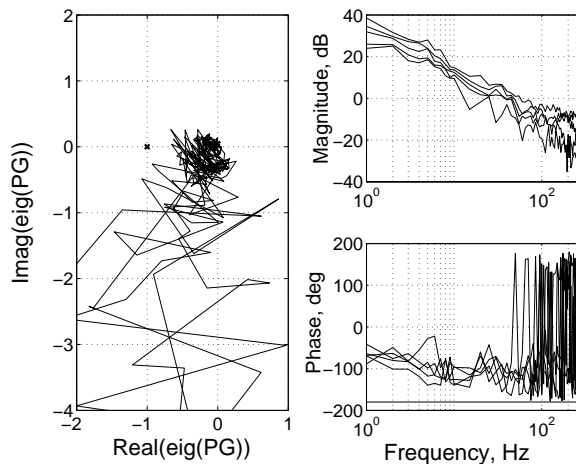


Fig. 9. Eigenvalues of measured $P(s)G(s)$.

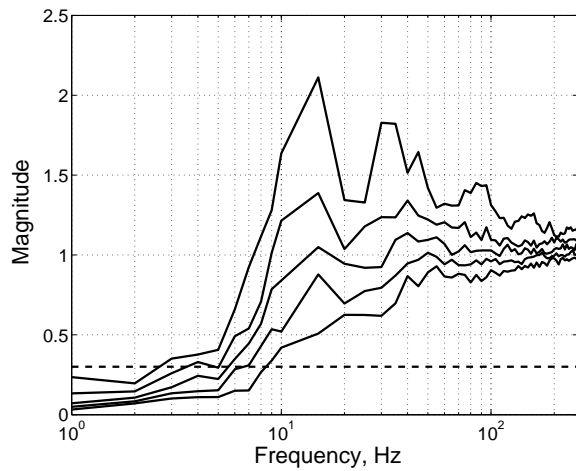


Fig. 10. Singular values of measured $(T(s) - I)$ for the MIMO controller.

where the gain is $k = 0.85$, the poles are $p_1 = 1.2\pi$ rad/sec, $p_2 = 100 \cdot 2\pi$ rad/sec, and $p_3 = 200 \cdot 2\pi$ rad/sec, the zero is $z_1 = 30 \cdot 2\pi$ rad/sec, the natural frequencies are $\omega_1 = 17 \cdot 2\pi$ rad/sec, $\omega_2 = 55 \cdot 2\pi$ rad/sec, $\omega_3 = 100 \cdot 2\pi$ rad/sec, and the damping ratios are $\zeta_1 = 0.2$ and $\zeta_2 = 0.5$.

This continuous scalar compensator is discretized using $z = e^{st_s}$ and matching DC gains (see *e.g.*, Franklin *et al.*, (1990)).

6. MEASURED RESULTS

Figure 9 shows the Nyquist and Bode plots for the open-loop frequency response, measured as the relation between force errors to measured forces in the hardware implementation. The actual gain margin is about 5 dB, and the phase margin is about 20 degrees.

Figure 10 shows the singular values of $(T(j\omega) - I)$ for the MIMO controller. These singular values are ideally 0. Although the isotropic bandwidth for the MIMO controller is about 3 Hz, it can be seen that the singular values of $(T(j\omega) - I)$ are much smaller for the MIMO

control case than for the SISO control case (see Figure 5) for frequencies up to 7 Hz. Hence force tracking is greatly improved in the 0–7 Hz range.

The large singular value of $(T(j\omega) - I)$ at about 15 Hz reflects a peak of $T(j\omega)$ of about 6 dB. The MIMO results are a very large improvement over SISO design results. The “feel” of the interface under the new control scheme is noticeably sharper, free space feels freer, and virtual walls are stiffer with less directional distortion.

7. CONCLUSION AND FUTURE WORK

We have developed a multivariable modeling and control strategy that leads to a simple control law which significantly increases the bandwidth of isotropic force transmission over SISO designs. Future work includes an evaluation of the robustness of this scheme as the hand is moved from the nominal position upon which the modeling and control design was based.

REFERENCES

- [1] Bellman, R. (1970). *Introduction to Matrix Analysis*, McGraw-Hill.
- [2] Bolanowski, S. J., G. A. Gescheider, R. T. Verrillo, and C. M. Checkosky (1988). “Four Channels Mediate the Mechanical Aspects of Touch,” *J. Acoust. Soc. Am.*, 84(5): 1680–1694.
- [3] Franklin, G. F., J. D. Powell, and M. L. Workman (1990). *Digital Control of Dynamic Systems*, Addison-Wesley.
- [4] Lawrence, D. A., C. D. Lee, L. Y. Pao, and R. Y. Novoselov (2000). “Shock and Vortex Visualization Using a Combined Visual/Haptic Interface,” *Proc. IEEE Visualization Conf.*, Salt Lake City, UT, pp. 131–137 and p. 548 (color plate).
- [5] Lee, C. D., D. A. Lawrence, and L. Y. Pao (2000). “A High-Bandwidth Force-Controlled Haptic Interface,” *Proc. ASME Dynamic Systems and Control Division*, DSC-Vol. 69–2, Orlando, FL, pp. 1299–1308.
- [6] Lee, C. D. (2002). *Modeling Mechanism and Hand Impedances for Improved Control of Haptic Interfaces*, Ph.D. Dissertation, Dept. of Elec. Eng., Univ. of Colorado.
- [7] Lee, C. D., D. A. Lawrence, and L. Y. Pao (2002). “Dynamic Modeling and Parameter Identification of a Parallel Haptic Interface,” *Proc. 10th Symposium on Haptic Interfaces for Virtual Environment and Teleoperator Systems, IEEE Virtual Reality Conf.*, Orlando, FL, pp. 172–179.
- [8] Ljung, L. (1987). *System Identification: Theory for the User*, Prentice-Hall.
- [9] MacFarlane, A. G. J. and I. Postlethwaite (1977). “The Generalized Nyquist Stability Criterion and Multivariable Root Loci,” *Int. J. Control*, 25(1): 81–127.
- [10] Skogestad, S. and I. Postlethwaite (1996). *Multivariable Feedback Control Analysis and Design*, Wiley.